Function and Connectivity in Human Primary Auditory Cortex: A Combined fMRI and DTI Study at 3 Tesla

Jaymin Upadhyay[1,2], Mathieu Ducros[1], Tracey A. Knaus[3,4], Kristen A. Lindgren[3,4], Andrew Silver[3,4], Helen Tager-Flusberg[3,4] and Dae-Shik Kim[1,3]

[1]Center for Biomedical Imaging, Department of Anatomy and Neurobiology, Boston University, School of Medicine, 715 Albany St., X-B01, Boston, MA, USA, [2]Program in Neuroscience, Boston University, 5 Cummington St., Boston, MA, USA, [3]Department of Anatomy and Neurobiology, Boston University School of Medicine, 715 Albany St., L-1004, Boston, MA, USA and [4]Lab of Developmental Cognitive Neuroscience, Department of Anatomy and Neurobiology, Boston University School of Medicine, 715 Albany St., L-814, Boston, MA, USA

Human primary auditory cortex (PAC) is functionally organized in a tonotopic manner. Past studies have used neuroimaging to characterize tonotopic organization in PAC and found similar organization as that described in mammals. In contrast to what is known about PAC in primates and nonprimates, in humans, the structural connectivity within PAC has not been defined. In this study, stroboscopic event-related functional magnetic resonance imaging (fMRI) was utilized to reveal mirror symmetric tonotopic organization consisting of a high–low–high frequency gradient in PAC. Furthermore, diffusion tensor tractography and probabilistic mapping was used to study projection patterns within tonotopic areas. Based on earlier physiological and histological work in nonhuman PAC, we hypothesized the existence of cross-field isofrequency (homotopic) and within-field nonisofrequency (heterotopic)–specific axonal projections in human PAC. The presence of both projections types was found in all subjects. Specifically, the number of diffusion tensor imaging (DTI) reconstructed fibers projecting between high- and low-frequency regions was greater than those fibers projecting between 2 high-frequency areas, the latter of which are located in distinct auditory fields. The fMRI and DTI results indicate that functional and structural properties within early stages of the auditory processing stream are preserved across multiple mammalian species at distinct evolutionary levels.

Keywords: diffusion tensor tractography, functional MRI, human auditory cortex, mirror symmetric, tonotopy

Introduction

Tonotopic organization is known to be present in nonprimates, nonhuman primates, and human auditory cortices (Merzenich and Brugge 1973; Merzenich et al. 1973; Morel and Kaas 1992; Morel et al. 1993; Heil et al. 1994; Harrison et al. 1996; Kaas and Hackett 2000; Engelien et al. 2002; Formisano et al. 2003; Lee, Imaizumi, et al. 2004; Lee, Schreiner, et al. 2004; Talavage et al. 2004; Lee and Winer 2005; Philibert et al. 2005; Petkov et al. 2006). Electrophysiological recordings in monkey auditory cortex suggest a "core" region consisting of 2 tonotopically organized fields (Merzenich and Brugge 1973; Merzenich et al. 1973; Morel et al. 1993; Kaas and Hackett 2000). The monkey auditory core is comprised of a primary field (A1) and a primary-like field R located adjacent and rostrolateral to A1 (Fig. 1). In cat auditory cortex there is a primary auditory field A1 and an adjacent field, anterior auditory field (AAF), which is also tonotopically organized. A third core region Rostrotemporal (RT) has also been identified in primates; however, physiological and anatomical properties are not as well established as in A1 and R. Within A1, clusters of auditory neurons (isofrequency

bands) located in the caudal-most regions possess best frequency responses (BFRs) to high frequencies, whereas those in rostral A1 have BFRs to low frequencies. In R, a tonotopic progression is also present; however, isofrequency bands located in caudal R are narrowly tuned to low frequencies and those located in rostral R respond best to high frequencies. Additionally, there is a slight tonotopic gradient in the medial–lateral direction in both core regions. These combined BFR characteristics of A1 and R yield mirror symmetric tonotopic maps oriented in the caudomedial and rostrolateral direction.

Many studies have corroborated and refined the tonotopic organization as described originally by Merzenich and Brugge (1973), and have also detailed the connectivity present in the auditory cortex in nonhuman primates and nonprimates (Merzenich et al. 1973; Galaburda and Sanides 1980; Galaburda and Pandya 1983; Seltzer and Pandya 1989; Morel et al. 1993; Kaas and Hackett 2000; Hackett et al. 2001; Padberg et al. 2003; Lee, Imaizumi, et al. 2004; Lee, Schreiner, et al. 2004; Lee and Winer 2005). From these prior studies it is known that the primary auditory fields have unique contralateral (commissural) and ipsilateral connectivity patterns in comparison with the primary visual (V1) and somatosensory (3b) fields (Fitzpatrick and Imig 1980; Galaburda and Pandya 1983; Krubitzer and Kaas 1990; Morel and Kaas 1992; Morel et al. 1993; Stepniewska et al. 1993; Casagrande and Kaas 1994; Jones et al. 1995). In terms of contralateral connections in V1 and 3b, it has been observed that there is little or no commissural connectivity throughout these 2 primary sensory regions, whereas ipsilateral axonal projections of V1 and 3b terminate widely to multiple higher level and distant areas. Conversely, commissural axonal projections amongst contralateral primary auditory regions are present. More specifically, axonal projections starting in A1 or R terminate in tonotopically matched core regions within the contralateral auditory cortex. With respect to ipsilateral axonal projections, there is strong and dense connectivity amongst primary and primary-like auditory regions. The distinct contralateral and ipsilateral auditory connectivity patterns probably indicate that each core region may have a substantial influence on the functional behavior of other core regions that respond differently to similar auditory stimuli.

Multiple animal studies have combined neurophysiologic and anatomical techniques to examine ipsilateral connectivity within tonotopically defined areas in auditory cortex (Merzenich and Brugge 1973; Merzenich et al. 1973; Fitzpatrick and Imig 1980; Imig and Reale 1980, 1981; Reale and Imig 1980; Morel and Kaas 1992; Morel et al. 1993; Thomas et al. 1993; Heil et al. 1994; Harrison et al. 1996; Lee, Imaizumi, et al. 2004; Lee, Schreiner,
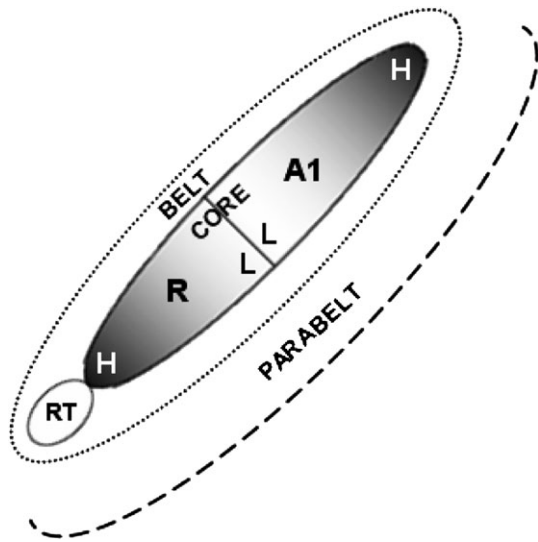
Figure 1. Tonotopic organization in monkey auditory core. The auditory core (A1, R, RT) is surrounded by belt and parabelt fields. High frequencies (H) are represented caudally in A1 and rostrally in R. Low frequencies (L) are represented rostrally in A1 and caudally in R. Tonotopic organization in RT is not clearly known.

et al. 2004; Lee and Winer 2005; Philibert et al. 2005). In one notable study in macaque monkey auditory cortex, Morel et al. (1993) performed tracer injections wheat germ agglutinin-horseradish peroxidase within an A1 high isofrequency contour. The majority of projections from the site of tracer injection was intrinsic and along the isofrequency contours in A1, whereas the second highest density of projections occurred to a tonotopically matched region in R. Similarly, tonotopic mapping and more sensitive tracer studies were performed in cat auditory cortex in a series of recent studies by Lee, Imaizumi, et al. (2004; Lee, Schreiner, et al. 2004; Lee and Winer 2005). Here low-to-high and high-to-low tonotopic gradients were observed in A1 and AAF, respectively, and similar ipsilateral connectivity patterns as those previously described by Morel et al. were obtained. For example, Cholera Toxin Beta (CTβ) injections made in a 3-kHz isofrequency contour of A1 yielded both a high density of homotopic and heterotopic labeling within A1, whereas cross-field homotopic and heterotopic labeling occurred between A1 and AAF at a much lesser extent. A similar labeling pattern was depicted when a Cholera Toxin Beta Gold (CTβG) injection was made in AAF.

The focus of the present study is on the characterization of ipsilateral connectivity patterns in human PAC in vivo, and how these axonal projection patterns within tonotopically defined areas compare with those previously described in histological work performed in nonhuman primates and nonprimates. Language processing is considered to be a highly complex auditory perception task in comparison with the perception of other human and many nonhuman sounds present within the environment. The exact nature of how the need to process language has possibly modified brain structures at the various levels of the auditory processing stream is not clearly known. However, with respect to the functional properties at the primary level of the auditory processing stream, the tonotopic organization present within human PAC is known to be similar between nonprimates, nonhuman primates, and humans. Recent functional magnetic resonance imaging (fMRI) work performed by Formisano et al. (2003) and Talavage et al. (2004) has

shown PAC activation maps similar to the mirror symmetric tonotopic organization as revealed by electrophysiological recordings in macaque monkeys as well as intracranial electrophysiological recording in humans (Liegeois-Chauvel et al. 1991, 1994; Kaas and Hackett 2000). Taking into consideration that analogous mirror symmetric tonotopic organization in PAC is present across the mammalian evolutionary scale, it is hypothesized that the connectivity patterns within the PAC are also predominately preserved amongst nonprimate mammals, nonhuman primates, and humans.

Several groups have utilized neuroimaging techniques as a means to noninvasively detail tonotopy in humans (Romani et al. 1982; Lauter et al. 1985; Pantev et al. 1988, 1995; Tiitinen et al. 1993; Verkindt et al. 1995; Howard et al. 1996; Wessinger et al. 1997; Bilecen et al. 1998; Hoke et al. 1998; Rosburg et al. 1998; Lockwood et al. 1999; Engelien et al. 2002; Schonwiesner et al. 2002; Formisano et al. 2003; Talavage et al. 2004; Philibert et al. 2005). These studies have depicted spatially distinct activity based on responses to tones varying in frequency, and some studies have shown mirror symmetric tonotopic organization as depicted in macaque monkey and cat auditory cortex.

To characterize ipsilateral connectivity in human PAC we performed stroboscopic event-related fMRI at 3 Tesla to obtain mirror symmetric tonotopic organization within the human PAC in each subject. By combining 2D anatomical and 3D surface-based functional image analysis in conjunction with diffusion tensor fiber tractography and probabilistic mapping, the axonal projection patterns present within tonotopically defined areas were characterized and quantified in vivo.

Methods

Subjects
Approval for this study was obtained from the Institutional Review Board of Boston University School of Medicine. Data were collected from 8 healthy right-handed subjects; 5 males, and 3 females, who were between the ages of 24 and 40 years. Informed consent was obtained from each volunteer prior to the scanning session.

MRI Parameters
All imaging data were collected using a 6-channel SENSE receiver coil on a 3-Tesla Philips Intera (Philips Medical Systems, Cleveland, OH) scanner housed with 2.2-g/cm maximum gradient strength. fMRI parameters: pulse sequence = field echo-echo planar image (EPI), time repetition/time echo (TR/TE) = 25 000/35 ms, imaging resolution = $1.8 \times 1.8 \times 2.0$ mm^3, flip angle = 90°, # of axial slices ~35. Structural MRI parameters: pulse sequence = 3D magnetization prepared rapid gradient echo, TR/TE = 7.47/3.4 ms, flip angle = 8.0°, imaging resolution = $0.9 \times 0.9 \times 1$ mm^3, # of axial slices ~160. Diffusion tensor imaging (DTI) parameters: pulse sequence = single-shot spin echo-EPI, TR/TE = 10 646/91 ms, b-value = 1069 s/mm^2 imaging resolutions = $1.8 \times 1.8 \times 2.0$ mm^3, # of diffusion directions = 15, # of axial slices ~73. Two DTI data sets were acquired for each subject. The 2 data sets were corrected for motion that results in interslice misregistration, coregistered, and averaged within and between acquisitions using Philips software (Philips Medical Systems).

Auditory Stimuli
Subjects were binaurally presented with 6 pure tones varying in frequency (0.3, 0.5, 0.8, 1, 2, and 3 kHz). The sound intensity was set to approximately 70-dB sound pressure level for each subject. All pure tones were created and presented at the same settings and had the same amplitude. No other normalization was performed. The specific frequencies were used in order to replicate and corroborate the results of a similar and recent study, which characterized mirror symmetric maps (Formisano et al. 2003). Humans have the ability to detect frequencies between 20 and 20 000 Hz.

All auditory stimuli were 1.8-s sine wave pure tones and were presented using standard MRI-compatible pneumatic headphones (Philips Medical Systems). The use of pneumatic headphones can lead to sound attenuation, particularly for higher frequencies. Nonetheless, the attenuation of the high frequencies did not occur to an extent such that auditory stimuli had significantly diminished sound quality, or to the extent where high frequencies sounded differently in comparison with when heard through conventional electronic speakers or headphones. The use of the MRI-compatible headphones enabled a sound attenuation of approximately 20 dB from the gradient acoustic noise. Furthermore, additional dense cushioning was put between the SENSE coil and MRI-compatible headphones to limit head movement. This cushioning provided additional attenuation of sound from gradient acoustic noise. The total sound attenuation was approximately 30 dB.

fMRI Data Collection

Functional imaging was performed using a stroboscopic event-related design (Belin et al. 1999; Hall et al. 1999). This technique allowed us to isolate the blood oxygen level–dependent (BOLD) response elicited by the auditory stimulus (pure tones) from the BOLD response brought about by the gradient acoustic noise of the MRI scanner. This technique has been utilized in previous auditory fMRI studies; however, the specific imaging parameters used in our study were optimized to yield the better fMRI activation maps, which resemble mirror symmetric tonotopic organization.

The BOLD response curve resulting from each pure tone was sampled in a pseudorandomized manner at 8 distinct time points (2, 3, 4, 6, 7, 8, 9, and 11 s). One baseline scan, where no sound was presented, was obtained in each functional run prior to the BOLD response curve sampling. An 11-s time interval in each epoch was allotted to allow for the full decay of the BOLD response resulting from gradient acoustic noise of the MRI scanner.

fMRI and Anatomical Data Analysis

BrainVoyager QX 1.6 software was utilized for single subject fMRI and anatomical image analysis (Brain Innovation, Maastricht, The Netherlands). fMRI data sets were preprocessed with a 3D head motion correction procedure, and low pass filtered to remove a linear trend cause by the long TR; thus increasing the signal-to-noise ratio (SNR). Anatomical images were interpolated up to a $1 \times 1 \times 1$ mm^3 isovoxel resolution and transformed into the Talairach coordinate system. Once white matter segmentation of the anatomical data sets was accomplished, the cortical surface was inflated using an automatic brain inflation algorithm. The fMRI data set for each subject was then coregistered to individual 2D anatomical images and 3D inflated brains. This allowed for the viewing of best frequency or tonotopic maps on anatomical data sets.

The presence of tonotopic organization in PAC was investigated by creating best frequency maps for each subject. First, statistical activation maps were obtained by computing a general linear model, where 6 predictors, one designated for each of the 6 frequency varying pure tones presented during a scanning session, were convoluted with the total BOLD response curve. For each subject activated regions were those regions with activated voxels above a significance of $P < 0.01$. Some subjects had a very strong response to the tones, which were presented. In these cases, the significance level was $P < 0.0001$ across all BOLD responses. Therefore, the significance level across frequencies was always the same for each subject but varied slightly across subjects. For every voxel with a significant response to the pure tones, the best frequency for that cortical region was estimated as the frequency at which the BOLD responses had the highest magnitude in comparison with the baseline. Due to the limited spatial resolution of BOLD fMRI at 3 Tesla, responses were grouped as being either low-frequency (0.3, 0.5, 0.8, and 1 kHz) or high-frequency (2 and 3 kHz) responses. Finally, best frequency regions or tonotopic maps were represented on 2D anatomical and 3D inflated representation of the brain by implementing a 2-color coding scheme; high-frequency maps were represented in dark blue, whereas low-frequency maps were represented in a light blue-green color.

DTI and Probabilistic Fiber Tracking Data Analysis

Single subject DTI and fiber tracking analyses were performed using BEAR, an in-house MATLAB based software package (Mathworks Inc.,

Natick, MA). EPI-based statistical maps were created in the BrainVoyager QX 1.6 environment, where each map represented either a high- or low-frequency response. Statistical maps along with the respective EPIs were then coregistered with a combined non-Talairach DTI and anatomical data set. This enabled high- and low-frequency specific regions of interest (ROIs) to be created in the combined DTI and anatomical data sets. All DTI, fMRI, and anatomical data sets were manually coregistered using the corpus callosum as well as the right and left lateral sulci as landmarks. High- and low-frequency ROIs were predominately confined to gray matter. We extended them to include approximately 3 voxels in the underlying white matter. When ROIs were initially created, these ROIs consisted of primarily gray matter. Prior to fiber tracking and probabilistic mapping these ROIs were extended into white matter to the extent of 2–3 voxels ($1.8 \times 1.8 \times 2.0$ mm^3). With respect to the activated gray matter, extension of the ROIs was in the inferior, posterior, and/or anterior directions. These ROIs were then used as seeding points for fiber tracking allowing axonal projections to be identified.

Streamline fiber tracking was performed using the INERTIA algorithm. INERTIA is based on the method described by Basser et al. (2000). At any point along the fiber tract a continuous interpolation of the diffusion tensor is used to determine the local fiber tangential orientation. The fiber is then propagated in straight line over a step size of one using the first order Euler method. The fiber propagation is terminated when the fractional anisotropy (FA) is smaller than 0.3, or the angle between successive fiber directions is greater than 60°. A high seeding point density of 27/voxel was used to generate a large number of fibers, thus increasing the chance of identifying any and all white matter pathways between 2 high-frequency ROIs or both high-frequency ROIs and low-frequency ROI. To view local axonal projections confined to the auditory cortex, fibers tracking was limited to axonal pathways connecting 2 ROIs. This enabled the characterization and quantification of fibers extending between 2 high-frequency ROIs or between high- and low-frequency ROIs. A multi-ROI connection analysis significantly reduces the creation of false fiber pathways due to the anatomical constraints imposed (see Discussion).

Probabilistic mapping of the identified axonal projections was achieved with the probabilistic fiber tracking method proposed by Parker et al. (2003). Probabilistic fiber tracking and mapping is performed by introducing uncertainty in the local fiber orientation at all points along its propagation using the standard Monte Carlo approach. Uncertainty in fiber orientation is described by the probability that it is deflected about its original vector e_1, given by the first eigenvector of the locally interpolated diffusion tensor. At each point along the fiber propagation, a random process is used to transform e_1 into e_1', where e_1' gives the new fiber orientation. Two rotations of angle σ and Φ are necessary to transform e_1 into e_1'. The probability density functions for Θ and Φ are defined in Parker et al. (2003); the smaller the FA, the greater the variability of Θ. In this study, 1000 fibers were generated from each starting point. We used the 0th order uncertainty model of Parker et al. (2003) with $\sigma_0 = 10°$, $\sigma_{max} = 50°$. The probability value for each voxel containing axonal projections was obtained by the equation $P = 100 \times N/\text{Nfibers}$ (in %), where N is the number of fibers going through a given voxel in the fiber bundle and Nfibers is the total number of fibers connecting both ROIs. Note that many fibers that are created in the Monte Carlo tracking method and that do not reach the target ROIs are not taken into account. In the equation above, no scaling is applied to probability maps. Probability maps are normalized to the total number of fibers, Nfibers. In the present work, we were interested in the connections between 2 frequency specific ROIs. Therefore, the probability maps computed using represent the fiber density in the bundle between the 2 ROIs and an indication of the most likely path between 2 ROIs. Lastly, the probability values, number DTI reconstructed of fibers (also referred to as "number of fibers"), fiber length, FA, average diffusivity (AD, [trace of the diffusion tensor]/3) were measured or calculated for high and low–high frequency fibers for each subject. Statistical analyses of group averaged fiber properties between the 2 fiber types were carried out using the student t-test (paired 2 sample for means). The corresponding 2-tailed P value, t-statistic (T), and degrees of freedom (df) are given for each statistical comparison.

Results

Mirror Symmetric Tonotopic Organization

Figures 2–4 show fMRI data for 3 subjects. In Figure 2, successive EPIs with combined high- and low-frequency BOLD activation maps are superimposed on corresponding T_1-weighted structural images for Subject 1. Both EPI and T_1-weighted image are axial slices of the left hemisphere in the non-Talairach coordinate system. Activation maps are present within the PAC, specifically along the transverse temporal gyrus (TTG) and transverse temporal sulcus (TTS). These successive images indicate good image quality for data obtained with the stroboscopic fMRI method.

Across all 8 subjects, high- and low-frequency responses were detected within PAC in left and right cerebral hemispheres and mirror symmetric tonotopic organization was looked for in both hemispheres. However, a clear presence of mirror symmetric tonotopic maps only occurred in one hemisphere in all 8 subjects. Of the 8 subjects, only in one subject was the presence of mirror tonotopic organization clearly defined in the right hemisphere instead of the left hemisphere. As a result all fMRI and DTI analyses were performed only in one hemisphere in each subject. A comparison of activation in right and left hemisphere PAC for Subject 2 is given in Figure 3A on an inflated brain surface. Here it can be seen that low and high frequencies activate distinct regions in the left hemisphere PAC and a clear mirror symmetric tonotopic map is present. High- and low-frequency BOLD response curves and BOLD activation maps projected on T_1-weighted sagittal images in the Talairach

coordinate system are shown in Figure 3B–D. Figure 3B and D depicts high-frequency activation clusters, in caudomedial PAC (Region B in Fig. 3A, –36, –33, –12) and rostrolateral PAC (Region D in Fig. 3A, –47, –21, 10), respectively. Figure 3C shows the low-frequency activation cluster (Region C in Fig. 3A, –40, –24, 12) between the caudomedial and rostrolateral high-frequency clusters. BOLD response curves for each high- and low-frequency activation cluster are shown. For both high-frequency clusters, it can be seen that the magnitude or % signal change in the BOLD responses for high-frequency pure tones (blue curves) is consistently higher than the BOLD response for low-frequency pure tones (red curves). In contrast, in Figure 3C the activated region has BOLD responses with greater % signal changes for low-frequency pure tones (red curves) than for high-frequency pure tones (blue curves). Statistical significance for activated regions depicted in Figure 3A–C was $P < 0.001$ to $P < 0.0001$.

BOLD activation maps for high- and low-frequency responses were projected onto an inflated brain representation of the left hemisphere in Talairach space to perform cortical surface-based functional analysis (Fig. 4). Figure 4A shows mirror symmetric tonotopic organization within the PAC for Subject 3. In the tonotopic map, 2 high-frequency regions were mapped: a caudomedial cluster (–33, –35, 16) and a rostrolateral cluster (–48, –16, 9). Between these 2 high-frequency mapped areas was a single low-frequency region (–42, –24, 12) oriented in the caudomedial–rostrolateral direction. Statistical significance for regions activated by high and low frequencies was at least $P < 0.001$.
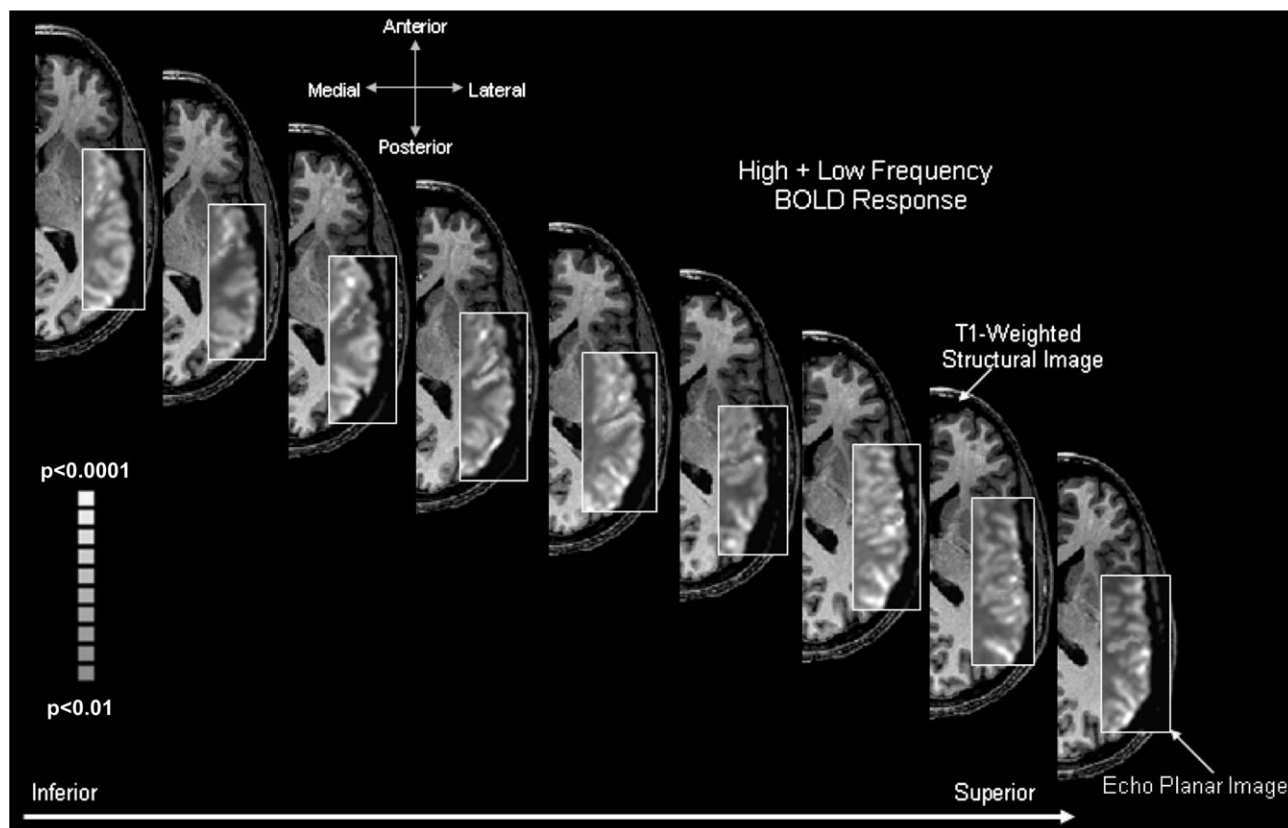

Figure 2. Two-dimensional activation maps on EP images for Subject 1. Left hemisphere EP images with BOLD activation maps are superimposed on T_1-weighted structural images in the non-Talairach coordinate system. These axial images indicate good image quality for data obtained with the stroboscopic event-related fMRI technique. EPI and T_1-weighted axial image are advanced from the inferior to superior direction.
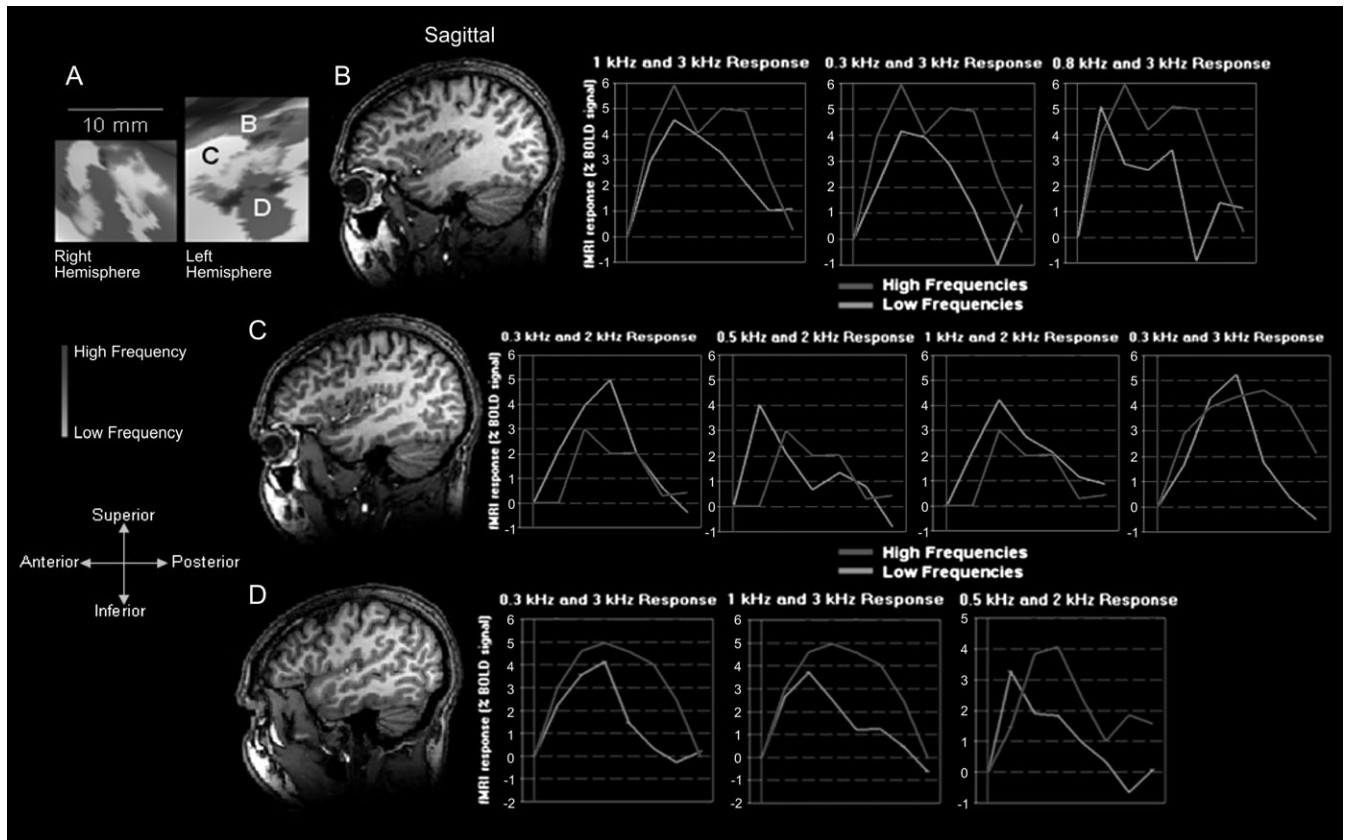
Figure 3. (*A–D*) Functional and anatomical data in Talairach coordinate system for Subject 2. (*A*) Comparison of activation maps in right and left PAC. Activation to high- and low-frequency pure tones was present in both cerebral hemispheres. However, a mirror symmetric map was only present in the left hemisphere and spanned a distance of 16.5 mm. High-frequency clusters are shown in dark blue, whereas the low-frequency response cluster is shown in light blue-green. LS, lateral sulcus; PSTG, posterior superior temporal gyrus. (*B–D*) Activation maps shown on 2D sagittal slices in Talairach coordinate system with high- and low-frequency BOLD response curves. (*B* and *D*) High-frequency activation clusters are located in caudomedial (*B*: −36, −33, −12) and rostrolateral (*D*: 47, −21, 10) regions of PAC. High-frequency (2 and 3 kHz, blue curve) BOLD responses for these 2 activation clusters have a higher % signal change than low-frequency (0.3, 0.5, 0.8 and 1 kHz, red curve) BOLD responses. (*C*) The low-frequency activation cluster (*C*: −40, −24, 12) is located in between the 2 high-frequency activation clusters. As in (*B*) and (*D*), low-frequency BOLD response curves are shown in red and high-frequency BOLD response curves are shown in blue.

Structural Connectivity in Tonotopic Regions

Figure 4*B* shows the high- and low-frequency activation clusters created in the coregistered T_1-weighted structural MRI and DTI data sets. These high- and low-frequency activation clusters were used as seeding points for fiber tractography and probabilistic mapping for Subject 2. Figures 5 and 6, respectively, illustrate representative data for high-frequency and low–high frequency fibers. Although high-frequency fibers (isofrequency-specific fibers) connect the caudomedial and rostrolateral high-frequency ROIs, low–high frequency fibers (nonisofrequency-specific fibers) project between the single low-frequency ROI with both high-frequency ROIs. In the full sagittal slice views (Figs. 5*A* and 6*A*) and in the enlarged views (Figs. 5*B* and 6*B*), both high and low–high frequency projections follow a similar caudomedial–rostrolateral orientation as the tonotopic organization of the PAC shown in Figure 4. For the low–high frequency projections, 2 local fiber groups were identified: one set of fiber projections in caudomedial PAC and another in rostrolateral regions. Furthermore, these fiber tracks were localized to white matter within the PAC (as determined by the presence of the TTG and TTS) or the posterior half of the superior temporal cortex.

Monte Carlo probabilistic mapping of the identified high and low–high frequency fibers allowed us to estimate fiber density within each white matter voxel (Figs. 5*C* and 6*C*). Those white matter regions coded in a light blue-green color represent a high density of fibers, whereas those coded in blue indicate white matter voxels possessing a lower fiber density. More specifically, those white matter regions colored in light blue-green have a higher percentage (~30 to 45%) of fibers that go through a given voxel in comparison with blue voxels, which have a lower percentage (~5 to 20%) of fibers.

High-frequency (Fig. 5*C*) and low–high frequency (Fig. 6*C*) probabilistic maps in conjunction with 2D representation of high- and low-frequency ROIs were superimposed and displayed on consecutive T_1-weighted sagittal slices for Subject 3. For Subject 3, the probability values for high and low–high frequency fiber bundles were 25.1 and 7.99, respectively. In each set of probabilistic maps, the first tile corresponds to the lateral most sagittal slice, where the extreme rostrolateral segments of the fiber bundle were present. Sagittal slices are advanced medially; thus the last tile depicts the probabilistic map of extreme caudomedial sections of the fiber bundle. High-frequency probabilistic maps comprised primarily light blue-green regions (~20 to 35%), therefore suggesting a high fiber density within the white matter fiber bundle. On the other hand, low–high frequency probabilistic maps were comprised primarily blue regions (~5 to 20%), therefore indicating a lower
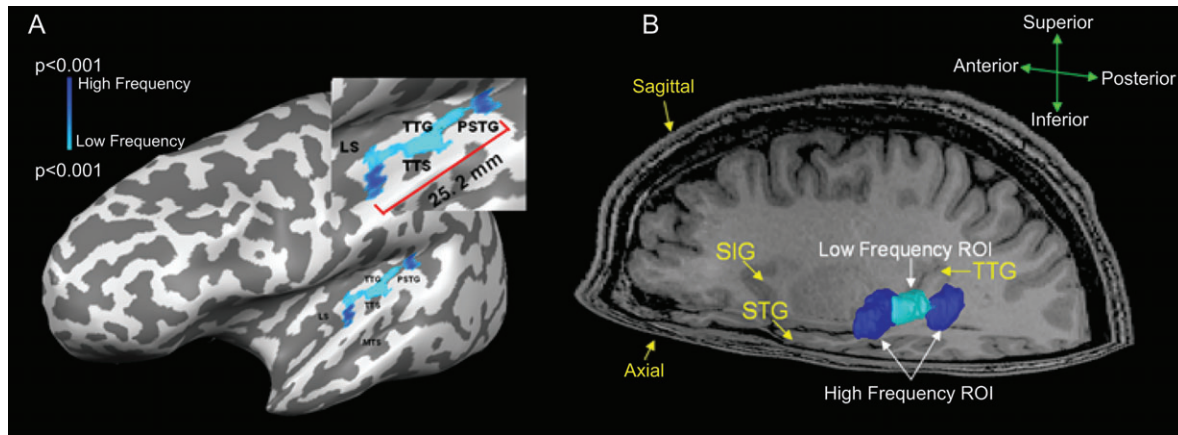
Figure 4. (*A* and *B*) Mirror symmetric tonotopic organization for Subject 3. (*A*) Tonotopic organization is shown on an inflated brain representation in the Talairach coordinate system. Two high-frequency regions were mapped within the PAC: a caudomedial cluster (−33, −35, 16) and a rostrolateral cluster (−48, −16, 9). Between these 2 high-frequency mapped areas was a low-frequency region (−42, −24, 12). Activation maps are present within the PAC, specifically along the TTG and TTS and spanned a distance of 25.2 mm. (*B*) Three-dimensional high- and low-frequency activation clusters were projected and created in coregistered T_1-weighted structural MRI and DTI data sets in the non-Talairach coordinate system. These 3D clusters were used as seeding points for fiber tractography and probabilistic mapping. High-frequency clusters are shown in blue, whereas the low-frequency cluster is represented in light blue-green. LS, lateral sulcus; PSTG, posterior superior temporal gyrus; STG, superior temporal gyrus; SIG, short insular gyrus.
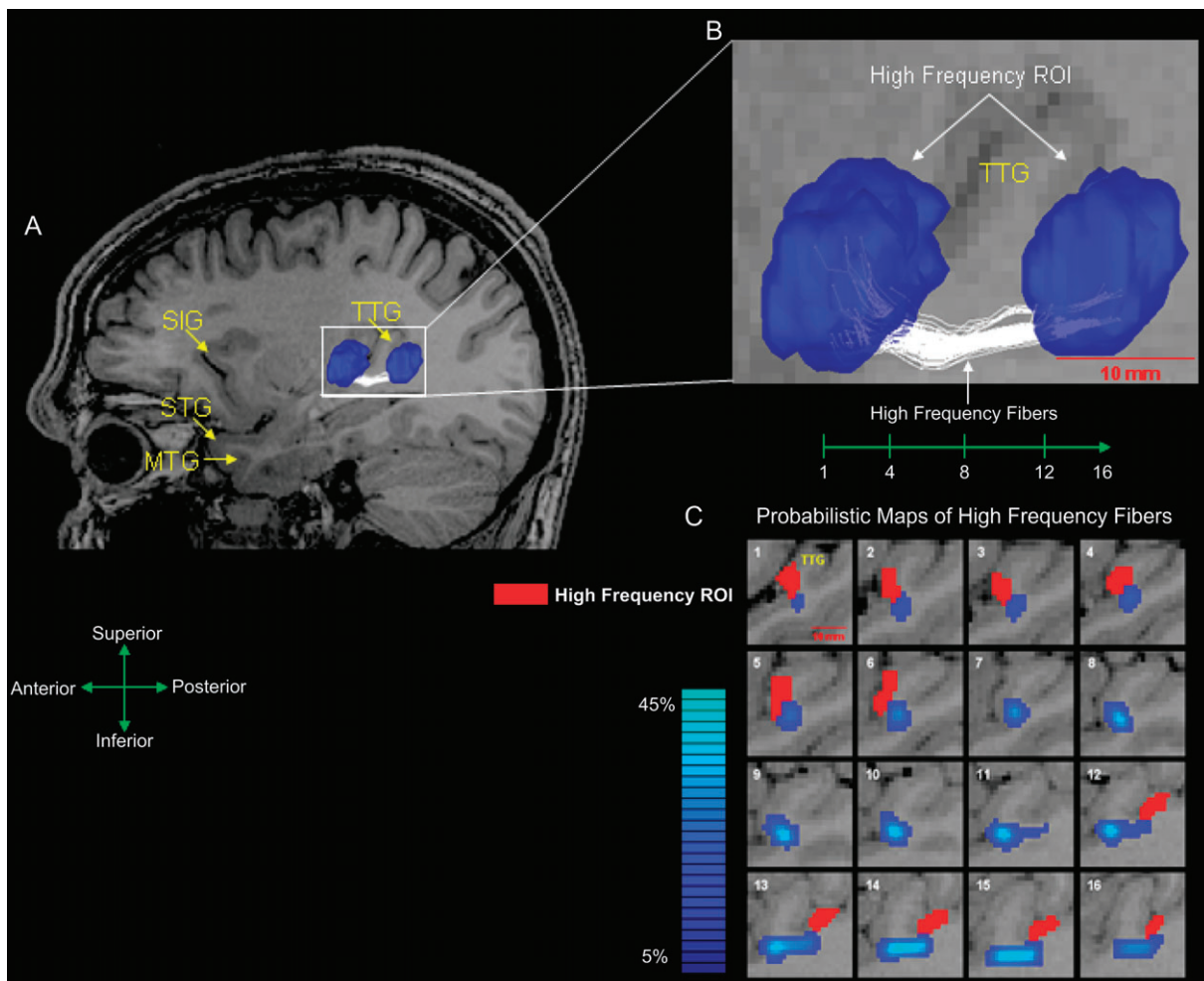

Figure 5. (*A–C*) High-frequency fibers (isofrequency-specific fibers) for Subject 3. (*A*) Fiber tracks connecting the caudomedial and rostrolateral high-frequency ROIs. (*B*) Zoomed view of a sagittal slice medial to high-frequency fibers and ROIs (represented in blue) shows the TTG in the background. (*C*) Probabilistic maps of this fiber bundle depict a fiber density in the range of 5–45%. Sagittal slices are advanced medially; thus the first tile represents the probabilistic map of the extreme rostrolateral section of the fiber bundle, and the last tile (#16) depicts the extreme caudomedial sections. *High fiber density = light blue-green voxels; low fiber density = dark blue voxels*. In the 2D sagittal slices with probabilistic maps, the gray matter regions of the high-frequency ROIs are shown in red. See Subject 3 in Figure 8*A* and *B* for probability and number of fibers value, respectively.
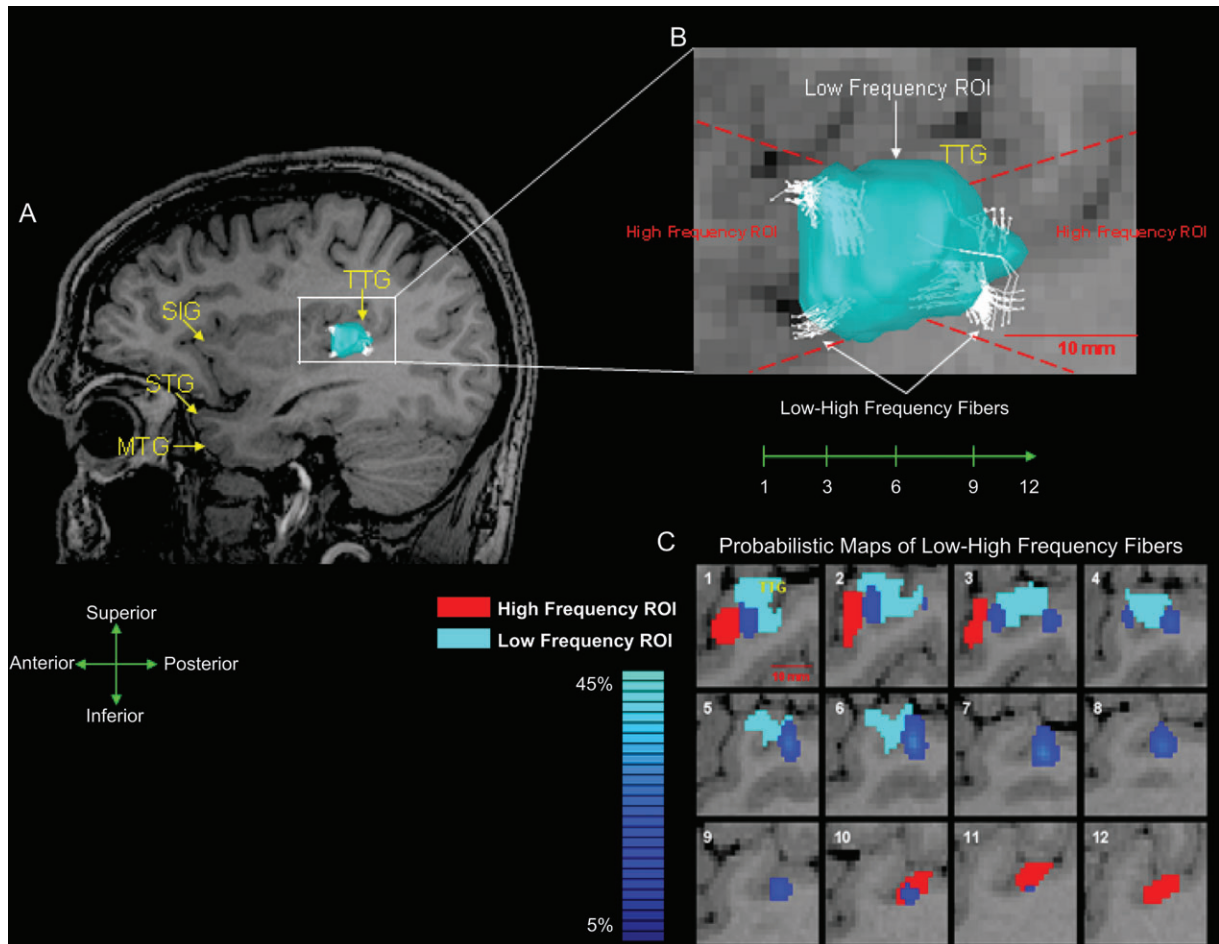
Figure 6. (A–C) Low–high frequency fibers (nonisofrequency-specific fibers) for Subject 3. (A) For low–high frequency projections, 2 distant fiber groups were identified; one set of fiber projections in caudomedial auditory cortex and another in rostrolateral regions. (B) Zoomed view of a sagittal slice medial to the low–high frequency fibers and low-frequency ROI (represented in light blue-green) shows the TTG in the background. Fibers project from the low-frequency ROI to high-frequency regions, which are located within the dashed red lines. (C) Probabilistic maps of these 2 fiber bundles depict a fiber density in the range of 5–25%. Sagittal slices are advanced medially; thus the first tile represents the probabilistic map of the extreme rostrolateral section of the rostrolateral fiber bundle and the last tile (#12) depicts the extreme caudomedial section of the caudomedial fiber bundle. In the 2D sagittal slices with probabilistic maps, the gray matter regions of the high-frequency ROIs are shown in red and the gray matter regions of the low-frequency ROI are shown in light blue-green. *High fiber density = light blue voxels; low fiber density = dark blue voxels.* See Subject 3 in Figure 8*A* and *B* for probability value and number of fibers value, respectively.

fiber density or more dispersed distribution of fibers in these bundles.

For Subject 2, high-frequency (Fig. 7*A*) and low–high frequency (Fig. 7*B*) probabilistic maps in conjunction with 2D representation of high- and low-frequency ROIs are superimposed and displayed on consecutive T_1-weighted axial slices. An image of the corresponding mirror symmetric tonotopic map is shown in Figure 7*C*. In Figure 7*A* and *B*, the first tile corresponds to the superior most axial slice, where the superior segments of the fiber bundle were present. Axial slices are advanced in the inferior direction; thus the last tile in Figure 7*A* and *B* depicts the probabilistic map of very inferior segments of the fiber bundle. As is the case in Subject 3, in Subject 2 the high-frequency fiber bundle (20.4) showed a higher probability value than the low–high frequency fiber bundle (5.71). This is a consistent trend for all subjects (Fig. 8*A*). It can clearly be seen that high-frequency fiber bundles possess a higher probability or higher fiber density than low–high frequency fiber bundles.

High-Frequency and Low–High Frequency Fiber Properties

Multiple fiber properties of high-frequency and low–high frequency (caudomedial plus rostrolateral fiber groups) fiber bundles were measured or calculated for each of the 8 subjects. In Figure 8*B* data are given for the total number of DTI reconstructed high and low–high frequency fibers for each subject. The total number of high-frequency fibers was much lower than the total number of low–high frequency fibers for all subjects. Group averaged data for high and low–high frequency fibers (mean ± standard error in mean) are given for length of fibers, FA, and AD (Fig. 9). In Figure 9*A*, it can be seen that the length of low–high frequency fibers (4 ± 0.6 mm) was significantly shorter than that of high-frequency fibers (14 ± 1.7 mm) ($P = 0.0008$, $T = 5.621$, df = 7). Group averaged diffusion properties for high and low–high frequency fibers are given in Figure 9*B* and *C*. The group averaged AD and FA between the 2 fiber types did not differ significantly. The FA of the high (0.46 ± 0.015) and low–high (0.41 ± 0.015) frequency fibers did
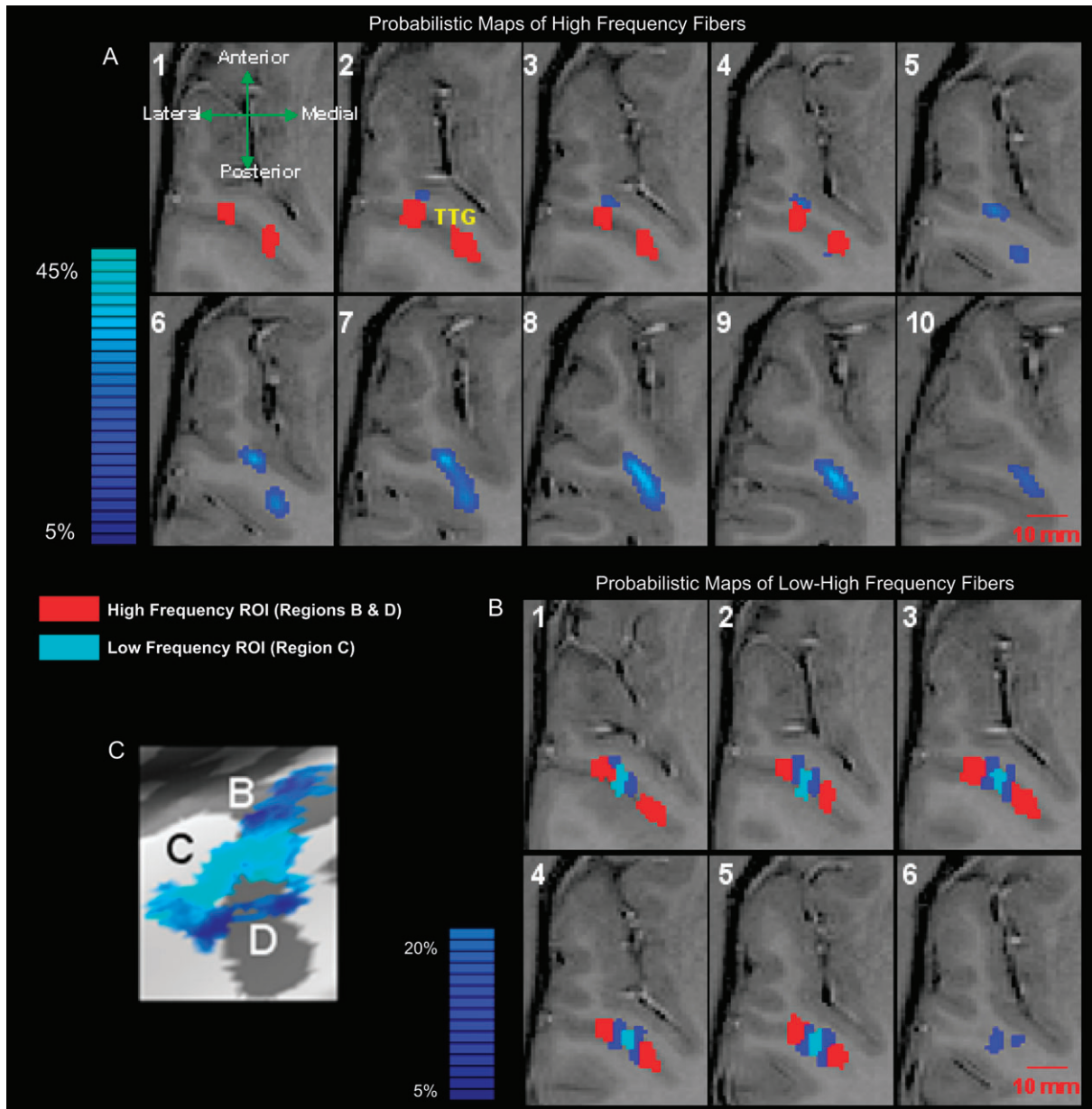
Figure 7. (*A* and *B*) Probabilistic maps for high frequency (isofrequency-specific fibers) and low–high frequency (nonisofrequency-specific fibers) for Subject 2 in the axial view. The very first tiles in show the superior most regions of the 1) probabilistic maps, 2) high-frequency ROIs (depicted in red), and 3) low-frequency ROI (depicted in light blue-green). Axial slices are advances in the inferior direction in both (*A*) and (*B*). Similar to Subject 3, it can be seen that the high-frequency probabilistic map has a higher probability value or fiber density than the low–high frequency probabilistic map. See Subject 2 in Figure 8*A* and *B* for probability and number of fibers value, respectively. *High fiber density = light blue-green voxels; low fiber density = dark blue voxels.*

not vary greatly (*P* = 0.0718, *T* = 2.120, df = 7). Similarly, the AD of high ((0.69 ± 0.053) × 10^3 mm²/s) and low–high ((0.61 ± 0.021) × 10^3 mm²/s) frequency fibers was similar amongst the 2 groups (*P* = 0.4023, *T* = 0.8915, df = 7). The critical *T*-value for all statistical tests was 2.365.

Discussion

Tonotopic White Matter Projection Patterns in Human Auditory Cortex

The present study is the first to characterize and quantify structural ipsilateral connectivity within human PAC in vivo.

This goal was achieved by implementing diffusion tensor tractography and probabilistic mapping in tonotopically defined areas. We investigated isofrequency-specific fiber tracks (Figs. 4 and 7*A*) projecting between 2 distant high-frequency ROIs (high-frequency fibers) as well as nonisofrequency-specific fiber tracks (Figs. 5 and 7*B*), which connect the single low-frequency ROI with both high-frequency ROIs (low–high frequency fibers). The combined caudomedial and rostrolateral low–high frequency fiber groups were found to have a significantly greater population of projections in comparison with high-frequency fibers (Fig. 8*B*); however, diffusion tensor probabilistic mapping shows that these nonisofrequency-specific fibers were more diffusely distributed along the low- and
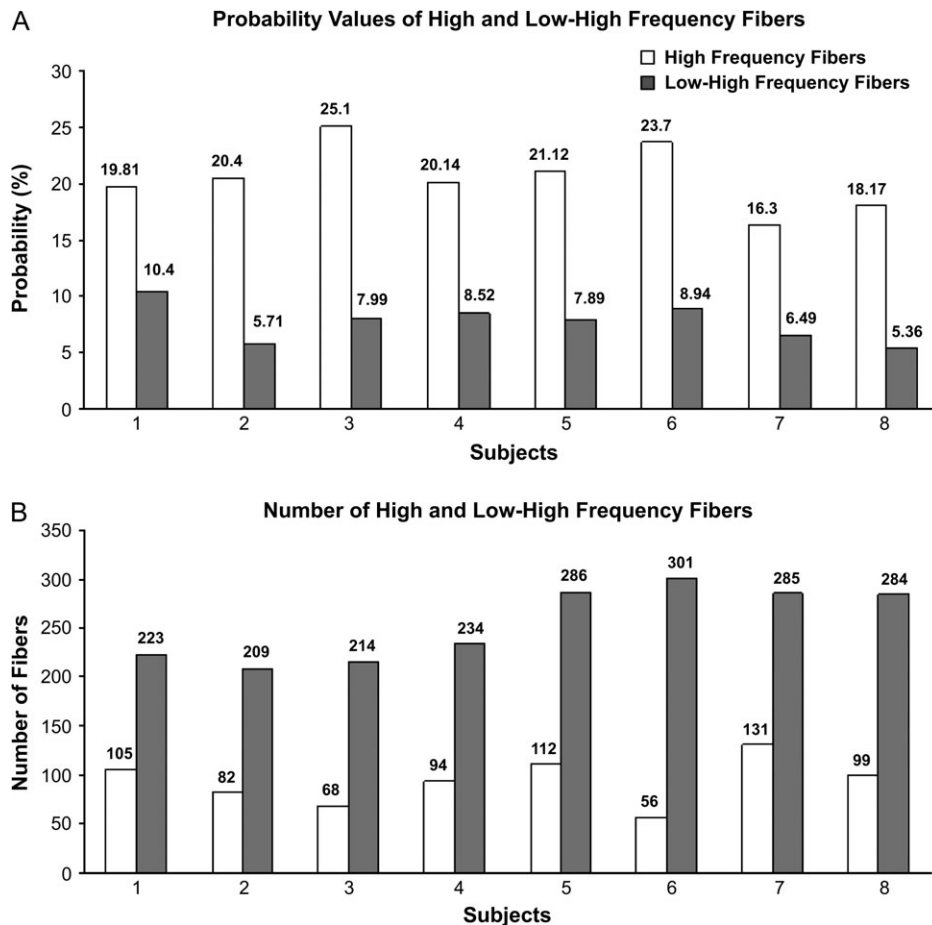
Figure 8. (*A* and *B*) Probability values and number of DTI reconstructed fibers for high and low–high frequency fiber bundles (caudomedial plus rostrolateral fiber groups) for all 8 subjects. (*A*) For each subject, the high-frequency fiber bundle has a much higher probability value or fiber density than the low–high frequency fiber bundles. (*B*) The number of low–high frequency fibers was more than twice as high as the number of high-frequency fibers across all subjects.

high-frequency border regions (Fig. 8*A*). In Figures 5*C* and 7*A*, probability maps of high-frequency fibers depict a single high-density white matter fiber bundle connecting the caudomedial and rostrolateral high-frequency ROIs. The exact functional implication(s) of the higher fiber density within the high-frequency fiber bundle is not known at this time. Furthermore, low–high frequency fibers were found to have a significantly shorter length than high-frequency fibers (Fig. 9*A*), whereas the diffusion properties, AD and FA, were similar amongst the 2 fiber groups (Fig. 9*B* and *C*). The results of similar AD and FA values were expected considering the fact that those diffusion properties (as measured by a 3 Tesla clinical scanner) do not vary greatly within a small and local white matter region of healthy adult brains (Zhai et al. 2003). The slightly greater AD and FA values for high-frequency fibers could be a result of microstructural properties such as myelination or a higher fiber density of this particular fiber bundle as observed with probabilistic mapping (Barkovich 2000; Beaulieu 2002).

The diffusion tensor tractography and probabilistic mapping results of this neuroimaging study suggest that the human PAC consists of an axonal projection pattern similar to that which has been observed in earlier tracer studies in macaque monkey and cat auditory cortices. The ipsilateral caudomedial and rostrolateral low–high frequency fiber bundles described above are believed to correspond to the within-field nonisofrequency-

specific (heterotopic) projections of A1 and R of macaque monkey auditory cortex, or the within-field nonisofrequency-specific (heterotopic) projections of A1 and AAF found in cat auditory cortex (Morel et al. 1993; Lee, Schreiner, et al. 2004). On the other hand, cross-field axons projecting between 2 tonotopically matched (homotopic) regions contained in the adjacent primary or primary-like auditory fields are analogous to the ipsilateral isofrequency-specific (high-frequency) fibers of the human PAC depicted and quantified in Figures 5 and 7*B*, respectively. Our observation that short-length nonisofrequency-specific fibers located within the same auditory fields significantly outnumbered the long-range isofrequency-specific fibers located in distinct auditory fields, suggests that the majority of projections within the human PAC remain intrinsic to that auditory region. This finding is similar to histological observations in macaque monkey and cat auditory cortices, where the within-field heterotopic labeling occurred more frequently than cross-field homotopic labeling amongst primary or primary-like auditory fields.

What little is known about the intrinsic structural connectivity of the human auditory cortex is inferred from the previously mentioned histological research in mammals, and from a limited number of postmortem studies in human PAC (Galuske et al. 2000; Tardif and Clarke 2001). In the work of Galuske et al., interhemispheric asymmetries in microcircuitry
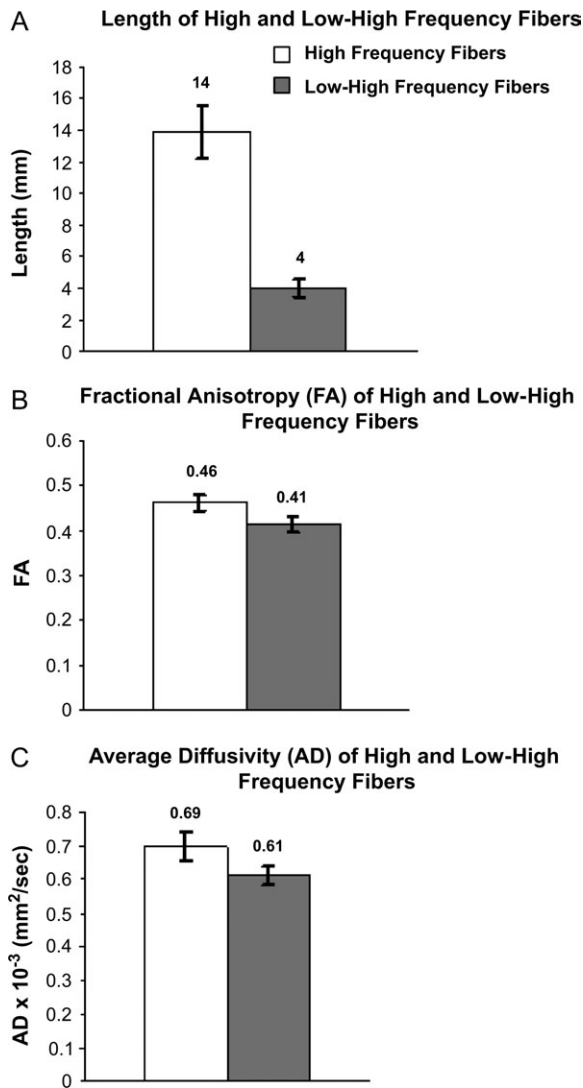
A Length of High and Low-High Frequency Fibers

□ High Frequency Fibers
■ Low-High Frequency Fibers

B Fractional Anisotropy (FA) of High and Low-High Frequency Fibers

C Average Diffusivity (AD) of High and Low-High Frequency Fibers

Figure 9. (*A–C*) Group-averaged (*n* = 8) fiber properties. (*A*) The length of low–high frequency fibers was significantly shorter than that of high-frequency fibers. (*B* and *C*) Both the AD and FA did not vary significantly amongst the high-frequency and low–high frequency fiber groups.

or columnar organization between right and left auditory regions were described. Here increased intercolumnar distance in the left posterior superior temporal gyrus was linked to the ability to process language at this hierarchical level; however, no asymmetries in intercolumnar distance were observed in PAC. Tardif and Clarke performed DiI injections to label axons in cytoarchitectonically defined areas of the auditory cortex. In the latter postmortem study, it was observed that axons within the TTG had a length that ranged between ~2–4 mm and projected to nearby auditory cortical units. This axonal length is close to the group averaged fiber length observed for low–high frequency fibers (4 ± 0.6 mm) of the present study; however, the fiber lengths of high-frequency projections (14 ± 1.7 mm) characterized above are much greater than the maximum axonal length of ~7 mm reported by Tardif and Clarke. The discrepancy in axonal length can be a due to a variety of factors such as 1) age range of subjects (present study: 24–40 years [*n* = 8]; and Tardif and Clarke: 67–94 years [*n* = 4]), 2) shrinkage caused by fixation of postmortem brains, or 3) exact gyral or

sulcal locations of where DiI tracer injections were made in comparison with the ROIs within auditory cortex used for tractography and probabilistic mapping. Nonetheless, in the combined electrophysiological and histological studies in macaque monkey, a tracer injection of HRP in an A1 high-frequency region (15–20 kHz) labeled a tonotopically matched region in R, which was approximately 12 mm from the A1 injection site (Morel et al. 1993). In the case of tracer studies in cat auditory cortex, this distance between 2 connected and tonotopically matched regions was approximately 6 mm (Lee, Schreiner, et al. 2004).

It has been shown in electrophysiological studies that although multiple auditory cortex regions can respond to the same auditory stimuli (have similar BFRs), other response properties can vary from one auditory field to another as well as within the same auditory field (Recanzone et al. 2004; Tian and Rauschecker 2004). These response properties can include but are not limited to intensity tuning and sensitivity, response latency, and/or frequency modulation selectivity. Therefore, structural connectivity within a single auditory field and among distinct auditory fields is necessary to integrate and process the various auditory features of sound. The connectivity patterns observed in this study provide evidence that similar structural connectivity patterns in primary and primary-like auditory fields exist in nonprimate mammals, nonhuman primates, and humans, thus enabling the integration of various sound properties. How structural connectivity differentiates at higher level auditory regions between humans and other mammalian species is not fully understood. Furthermore, very little is known about how the structural connectivity patterns amongst various temporal, parietal, and frontal cortical structures supports language processing. Characterization and quantification of axonal projections along the hierarchically organized language processing stream will be the focus of our future investigations.

Mirror Symmetric Tonotopic Organization

In this experiment, we demonstrated the ability to obtain mirror symmetric tonotopic organization using a 3-Tesla clinical scanner in healthy subjects. Prior to this study, several groups have utilized a magnetic field strength of 3 Tesla or below to elucidate frequency specific responses within the human PAC but activation maps did not resemble *mirror symmetric* tonotopic organization (Wessinger et al. 1997; Bilecen et al. 1998; Engelien et al. 2002; Schonwiesner et al. 2002). Numerous methodological differences between this study and past research may explain the tonotopic organization shown and described above (Figs. 3 and 4). Two such differences are the specific range and number of different frequencies presented and also the functional image analysis performed. Here 6 pure tones, ranging from 0.3 to 3 kHz were presented, and both 2D and 3D cortical surface-based functional analyses were carried out. Furthermore, we implemented an unconventionally long TR of 25 s within a stroboscopic event-related fMRI paradigm. This enabled the complete isolation of the BOLD responses arising from the pure tone stimuli from that caused by the ambient gradient noise.

Another aspect of our methodology that further enabled high- and low-frequency regions to be more clearly identified was the separation or binning of the BOLD responses to high-frequency pure tones (2 and 3 kHz) and low-frequency pure tones (0.3, 0.5, 0.8, and 1 kHz). We found that at 3 Tesla, there

was not sufficient SNR or contrast-to-noise ratio, and thus, spatial resolution in BOLD mapping to accurately specify where each pure tone is processed within the PAC. The spatial resolution, however, was sufficient to accurately localized BOLD responses for a range of frequencies. This is in contrast to a previous fMRI study that was the first to identify mirror symmetric tonotopic organization in human PAC and implemented a TR of 20 s within a stroboscopic event-related fMRI paradigm (Formisano et al. 2003). The study by Formisano et al. however, was performed on a 7-Tesla scanner equipped with far better gradient instrumentation than that available on conventional 3-Tesla clinical scanners. Whereas the gradient strength at 7 Tesla was 4 Gauss/cm, at 3 Tesla the gradient strength is 2.2 Gauss/cm. As a result, the spatial resolution of their high magnetic field BOLD fMRI study was superior to that of the present study (Yacoub et al. 2001; Pfeuffer et al. 2002; Ugurbil et al. 2003). However, the overall spatial layout and location of the mirror symmetric tonotopic maps shown on a cortical surface in Figures 3 and 4 are similar to those reported previously (Formisano et al. 2003; Talavage et al. 2004).

Technical Considerations

One shortcoming of the diffusion tensor tractography and probabilistic mapping techniques is the inability to distinguish if a group of fibers that emanate from region "a" to region "b" has an opposite projection scheme or if the fiber group represents a combination of both fiber trajectories. This is in contrast to anatomical techniques implemented in animal work. For example, in cat auditory cortex, axonal projection properties of fibers between A1 and AAF can be compared and contrasted with fibers projecting from AAF to A1. On a related note, with this technique quantifying homotopic labeling, which occurs within the same isofrequency contour or within the same ROI is not possible. This again is in contrast to past in vivo labeling studies, which have been described above. The limitation exists because of the fact that the entire isofrequency area (referred to in this work as the high-frequency or low-frequency ROI) is used as the seeding point for characterizing fiber projections. This latter limitation stems from the fact that there is low spatial resolution at 3 Tesla. In consequence, the present study was limited to characterizing and quantifying the fiber properties of cross-field isofrequency-specific fibers and within-field nonisofrequency-specific fibers.

Limited spatial resolution of conventional DTI and its applications performed at 3 Tesla also pose the problem of fiber crossing within a DTI voxel. This limiting factor, in turn can at times lead to erroneous fiber characterization and decrease the sensitivity of this technique (Tuch et al. 2003). Here diffusion tensor probabilistic mapping was used to validate and compliment the fiber projections identified using the "deterministic" technique of diffusion tensor tractography. It is noted that probabilistic mapping showed that fiber bundles consisted of at least a 5% probability, which corresponded to the lowest fiber density shown in Figures 5–7. By considering voxels within a fiber bundle with a probability of at least 5%, chances of observing false negative and false positive fiber pathways or voxels are lowered. Furthermore, by combining streamline fiber tracking with Monte Carlo probabilistic mapping we observed that the regions of highest fiber density or highest probability identified with probabilistic mapping are the same regions as the centers of high and low–high frequency

fiber bundles. The outer most regions of the high and low–high frequency fiber bundles showed slightly less dense regions but possessed a probability of at least 5%. The results of probabilistic mapping can yield a sense of how valid the results of streamline fiber tracking. If, for example, an identified fiber track has a probability of 1% or 2%, conclusions made about the fiber tract should be made with caution because the presence of such a loosely packed fiber bundle is unlikely.

To further decrease the likelihood of obtaining false fiber pathways, fiber tracking and probabilistic mapping were performed between 2 ROIs rather than a single ROI. If fiber tracking or probabilistic mapping is only done with a single ROI it is very often the case that one would obtain false fiber pathways. For example, what occurs if a single ROI in the TTG is used for fiber tracking and probabilistic mapping is that a false fiber pathway consisting of the arcuate fasciculus or inferior longitudinal fasciculus is created. It is known from postmortem studies in humans and nonhuman primates that fibers of PAC project to regions either within the PAC or to adjacent and surrounding higher order auditory regions. Furthermore, it is these higher order regions, such as the posterior superior temporal gyrus, that are the starting and ending points of fiber bundles such as the arcuate fasciculus. In fiber tracking or probabilistic mapping a fiber will be created as long as a voxel possesses the biophysical properties (FA, angle, or direction of principle eigenvector, etc.) that pass certain defined parameter threshold.

The presence of thalamocortical fibers projecting between tonotopic areas and the thalamus, commissural fibers projecting to the contralateral auditory cortex, and ipsilateral inter-ROI fibers was sought. Thalamocortical and commissural fibers were searched for by seeking all fibers generated from a single high- or low-frequency specific ROI. These pathways, however, were not identified in any of the 8 subjects (data not shown) when performing either streamline fiber tracking or Monte Carlo probabilistic mapping. The absence of these particular pathways is mostly likely a result of the extension of the fibers through complex white matter regions where crossing fibers are present. Other factors were voxels with low FA value (FA < 0.3) along the thalamocortical or commissural pathways, an angle greater than 60° between principle eigenvectors, or sufficient drop in SNR across these substantially long pathways. These fibers could possibly be identified using substandard fiber tracking parameters. However, implementing less stringent parameters would greatly increase the likelihood of identifying erroneous fiber pathways in addition to real pathways, thus making it difficult to accurately characterize and quantify thalamocortical and commissural pathways. Although Monte Carlo probabilistic mapping or similar methods can provide better and more accurate characterization of white matter pathways, implementation of DTI data acquisitions techniques such as high angular resolution diffusion imaging is what can possibly alleviate the crossing fiber dilemma. Therefore, this study was restricted to the examination of short distance ipsilateral pathways (~5–20 mm) within the auditory cortex where biophysical changes and the presence of crossing fibers occur at a lower extent.

Because of the limited spatial resolution available for BOLD fMRI mapping at 3 Tesla, we were not able to identify the exact spatial location of where in the auditory cortex each presented pure tone frequency was processed. Therefore, it was not possible to exactly specify a central low-frequency region similar to the low-frequency region defined in monkey (Morel

et al. 1993; Petkov et al. 2006) and human (Formisano et al. 2003) auditory cortices, or the central high-frequency region defined in cat auditory cortex (Lee, Schreiner, et al. 2004). The central most regions of these "common" low- or high-frequency areas are often the location of the border between A1 and R in monkey or A1 and AAF in cat. Such a clear division has yet to be defined in human PAC on the basis of combined cytoarchitectonic and functional findings. Recent work by Morosan et al. (2001) did show consistent cytoarchitectural variability throughout and along the human PAC (Te1) and subsequently segmented the region into Te1.1 (extreme lateral portion of Te1), Te1.0, and Te1.2 (extreme medial portion of Te1). Relationships amongst the observed cytoarchitectural variability to auditory functional responses were also postulated by Morosan et al. In the present study, a definite high–low–high tonotopic gradient was identified for each subject. Equally important is the fact that 2 *distant* (~10 mm or more) high-frequency regions or low–high frequency borders were present within each mirror symmetric tonotopic map; a further indication of similar frequency responses possibly occurring in 2 cytoarchitectural distinct regions.

In conclusion, this study characterized and quantified ipsilateral structural connectivity in human PAC in vivo. By combining functional and structural imaging we observed that the connectivity patterns in human PAC were similar to those that have been described in histological work carried out in macaque monkey and cat auditory cortex. The human PAC consists of significantly more nonisofrequency-specific projections than those which are isofrequency specific. Furthermore, performing stroboscopic fMRI and diffusion tensor tractography and probabilistic mapping is a suitable noninvasive technique to study structural connectivity within and amongst functionally defined areas in human auditory cortex.

Notes

Address correspondence to Dae-Shik Kim, PhD, Department of Anatomy and Neurobiology, 715 Albany Street, L-1004, Boston University School of Medicine, Boston, MA 02118, USA. Email: dskim@bu.edu.

References

Barkovich AJ. 2000. Concepts of myelin and myelination in neuroradiology. AJNR Am J Neuroradiol. 21:1099-1109.

Basser PJ, Pajevic S, Pierpaoli C, Duda J, Aldroubi A. 2000. In vivo fiber tractography using DT-MRI data. Magn Reson Med. 44:625-632.

Beaulieu C. 2002. The basis of anisotropic water diffusion in the nervous system—a technical review. NMR Biomed. 15:435-455.

Belin P, Zatorre RJ, Hoge R, Evans AC, Pike B. 1999. Event-related fMRI of the auditory cortex. Neuroimage. 10:417-429.

Bilecen D, Scheffler K, Schmid N, Tschopp K, Seelig J. 1998. Tonotopic organization of the human auditory cortex as detected by BOLD-FMRI. Hear Res. 126:19-27.

Casagrande VA, Kass JH. 1994. In: Peters A, Rockland K, editors. Cerebral Cortex. Vol. 10. New York: Plenum. p. 201-259.

Engelien A, Yang Y, Engelien W, Zonana J, Stern E, Silbersweig DA. 2002. Physiological mapping of human auditory cortices with a silent event-related fMRI technique. Neuroimage. 16:944-953.

Fitzpatrick KA, Imig TJ. 1980. Auditory cortico-cortical connections in the owl monkey. J Comp Neurol. 192:589-610.

Formisano E, Kim DS, Di Salle F, van de Moortele PF, Ugurbil K, Goebel R. 2003. Mirror-symmetric tonotopic maps in human primary auditory cortex. Neuron. 40:859-869.

Galaburda A, Sanides F. 1980. Cytoarchitectonic organization of the human auditory cortex. J Comp Neurol. 190:597-610.

Galaburda AM, Pandya DN. 1983. The intrinsic architectonic and connectional organization of the superior temporal region of the rhesus monkey. J Comp Neurol. 221:169-184.

Galuske RA, Schlote W, Bratzke H, Singer W. 2000. Interhemispheric asymmetries of the modular structure in human temporal cortex. Science. 289:1946-1949.

Hackett TA, Preuss TM, Kaas JH. 2001. Architectonic identification of the core region in auditory cortex of macaques, chimpanzees, and humans. J Comp Neurol. 441:197-222.

Hall DA, Haggard MP, Akeroyd MA, Palmer AR, Summerfield AQ, Elliott MR, Gurney EM, Bowtell RW. 1999. "Sparse" temporal sampling in auditory fMRI. Hum Brain Mapp. 7:213-223.

Harrison RV, Kakigi A, Hirakawa H, Harel N, Mount RJ. 1996. Tonotopic mapping in auditory cortex of the chinchilla. Hear Res. 100:157-163.

Heil P, Rajan R, Irvine DR. 1994. Topographic representation of tone intensity along the isofrequency axis of cat primary auditory cortex. Hear Res. 76:188-202.

Hoke ES, Ross B, Hoke M. 1998. Auditory afterimage: tonotopic representation in the auditory cortex. Neuroreport. 9:3065-3068.

Howard MA 3rd, Volkov IO, Abbas PJ, Damasio H, Ollendieck MC, Granner MA. 1996. A chronic microelectrode investigation of the tonotopic organization of human auditory cortex. Brain Res. 724:260-264.

Imig TJ, Reale RA. 1980. Patterns of cortico-cortical connections related to tonotopic maps in cat auditory cortex. J Comp Neurol. 192: 293-332.

Imig TJ, Reale RA. 1981. Ipsilateral corticocortical projections related to binaural columns in cat primary auditory cortex. J Comp Neurol. 203:1-14.

Jones EG, Dell'Anna ME, Molinari M, Rausell E, Hashikawa T. 1995. Subdivisions of macaque monkey auditory cortex revealed by calcium-binding protein immunoreactivity. J Comp Neurol. 362:153-170.

Kaas JH, Hackett TA. 2000. Subdivisions of auditory cortex and processing streams in primates. Proc Natl Acad Sci USA. 97:11793-11799.

Krubitzer LA, Kaas JH. 1990. The organization and connections of somatosensory cortex in marmosets. J Neurosci. 10:952-974.

Lauter JL, Herscovitch P, Formby C, Raichle ME. 1985. Tonotopic organization in human auditory cortex revealed by positron emission tomography. Hear Res. 20:199-205.

Lee CC, Imaizumi K, Schreiner CE, Winer JA. 2004. Concurrent tonotopic processing streams in auditory cortex. Cereb Cortex. 14:441-451.

Lee CC, Schreiner CE, Imaizumi K, Winer JA. 2004. Tonotopic and heterotopic projection systems in physiologically defined auditory cortex. Neuroscience. 128:871-887.

Lee CC, Winer JA. 2005. Principles governing auditory cortex connections. Cereb Cortex. 15:1804-1814.

Liegeois-Chauvel C, Musolino A, Badier JM, Marquis P, Chauvel P. 1994. Evoked potentials recorded from the auditory cortex in man: evaluation and topography of the middle latency components. Electroencephalogr Clin Neurophysiol. 92:204-214.

Liegeois-Chauvel C, Musolino A, Chauvel P. 1991. Localization of the primary auditory area in man. Brain. 114(Pt 1A):139-151.

Lockwood AH, Salvi RJ, Coad ML, Arnold SA, Wack DS, Murphy BW, Burkard RF. 1999. The functional anatomy of the normal human auditory system: responses to 0.5 and 4.0 kHz tones at varied intensities. Cereb Cortex. 9:65-76.

Merzenich MM, Brugge JF. 1973. Representation of the cochlear partition of the superior temporal plane of the macaque monkey. Brain Res. 50:275-296.

Merzenich MM, Knight PL, Roth GL. 1973. Cochleotopic organization of primary auditory cortex in the cat. Brain Res. 63:343-346.

Morel A, Garraghty PE, Kaas JH. 1993. Tonotopic organization, architectonic fields, and connections of auditory cortex in macaque monkeys. J Comp Neurol. 335:437-459.

Morel A, Kaas JH. 1992. Subdivisions and connections of auditory cortex in owl monkeys. J Comp Neurol. 318:27-63.

Morosan P, Rademacher,J, Schleicher A, Amunts K, Schormann T, Zilles K. 2001. Human primary auditory cortex: cytoarchitectonic

subdivisions and mapping into a spatial reference system. Neuro-image. 13:684–701.

Padberg J, Seltzer B, Cusick CG. 2003. Architectonics and cortical connections of the upper bank of the superior temporal sulcus in the rhesus monkey: an analysis in the tangential plane. J Comp Neurol. 467:418-434.

Pantev C, Bertrand O, Eulitz C, Verkindt C, Hampson S, Schuierer G, Elbert T. 1995. Specific tonotopic organizations of different areas of the human auditory cortex revealed by simultaneous magnetic and electric recordings. Electroencephalogr Clin Neurophysiol. 94:26–40.

Pantev C, Hoke M, Lehnertz K, Lutkenhoner B, Anogianakis G, Wittkowski W. 1988. Tonotopic organization of the human auditory cortex revealed by transient auditory evoked magnetic fields. Electroencephalogr Clin Neurophysiol. 69:160–170.

Parker GJ, Haroon HA, Wheeler-Kingshott CA. 2003. A framework for a streamline-based probabilistic index of connectivity (PICo) using a structural interpretation of MRI diffusion measurements. J Magn Reson Imaging. 18:242–254.

Petkov CI, Kayser C, Augath M, Logothetis NK. 2006. Functional imaging reveals numerous fields in the monkey auditory cortex. PLoS Biol. 4:e215

Pfeuffer J, van de Moortele PF, Yacoub E, Shmuel A, Adriany G, Andersen P, Merkle H, Garwood M, Ugurbil K, Hu X. 2002. Zoomed functional imaging in the human brain at 7 Tesla with simultaneous high spatial and high temporal resolution. Neuroimage. 17:272–286.

Philibert B, Beitel RE, Nagarajan SS, Bonham BH, Schreiner CE, Cheung SW. 2005. Functional organization and hemispheric comparison of primary auditory cortex in the common marmoset (Callithrix jacchus). J Comp Neurol. 487:391–406.

Reale RA, Imig TJ. 1980. Tonotopic organization in auditory cortex of the cat. J Comp Neurol. 192:265–291.

Recanzone GH, Beckerman NS. 2004. Effects of intensity and location on sound location discrimination in macaque monkeys. Hear Res. 198:116–124.

Romani GL, Williamson SJ, Kaufman L. 1982. Tonotopic organization of the human auditory cortex. Science. 216:1339–1340.

Rosburg T, Kreitschmann-Andermahr I, Emmerich E, Nowak H, Sauer H. 1998. Hemispheric differences in frequency dependent dipole orientation of the human auditory evoked field component N100m. Neurosci Lett. 258:105–108.

Schonwiesner M, von Cramon DY, Rubsamen R. 2002. Is it tonotopy after all? Neuroimage. 17:1144–1161.

Seltzer B, Pandya DN. 1989. Intrinsic connections and architectonics of the superior temporal sulcus in the rhesus monkey. J Comp Neurol. 290:451–471.

Stepniewska I, Preuss TM, Kaas JH. 1993. Architectonics, somatotopic organization, and ipsilateral cortical connections of the primary motor area (M1) of owl monkeys. J Comp Neurol. 330:238–271.

Talavage TM, Sereno MI, Melcher JR, Ledden PJ, Rosen BR, Dale AM. 2004. Tonotopic organization in human auditory cortex revealed by progressions of frequency sensitivity. J Neurophysiol. 91:1282–1296.

Tardif E, Clarke S. 2001. Intrinsic connectivity of human auditory areas: a tracing study with DiI. Eur J Neurosci. 13:1045–1050.

Tian B, Rauschecker JP. 2004. Processing of frequency-modulated sounds in the lateral auditory belt cortex of the rhesus monkey. J Neurophysiol 92:2993–3013.

Thomas H, Tillein J, Heil P, Scheich H. 1993. Functional organization of auditory cortex in the mongolian gerbil (Meriones unguiculatus). I. Electrophysiological mapping of frequency representation and distinction of fields. Eur J Neurosci. 5:882–897.

Tiitinen H, Alho K, Huotilainen M, Ilmoniemi RJ, Simola J, Naatanen R. 1993. Tonotopic auditory cortex and the magnetoencephalographic (MEG) equivalent of the mismatch negativity. Psychophysiology. 30:537–540.

Tuch DS, Reese TG, Wiegell MR, Weden VJ. 2003. Diffusion MRI of complex nerual architecture. Neuron. 40:885–895.

Ugurbil K, Toth L, Kim DS. 2003. How accurate is magnetic resonance imaging of brain function?. Trends Neurosci. 26:108–114.

Verkindt C, Bertrand O, Perrin F, Echallier JF, Pernier J. 1995. Tonotopic organization of the human auditory cortex: N100 topography and multiple dipole model analysis. Electroencephalogr Clin Neurophysiol. 96:143–156.

Wessinger CM, Buonocore MH, Kussmaul CL, Mangun GR. 1997. Tonotopy in the human auditory cortex examined with functional magnetic resonance imaging. Hum Brain Mapp. 5:18–25.

Yacoup E, Shmuel A, Pfeuffer J, Van De Moortele PF, Adriany G, Andersen P, Vaughan JT, Merkle H, Ugurbil K, Hu X. 2001. Imaging brain function in humans at 7 Tesla. Magn. Reson Med. 45:588–594.

Zhai G, Lin W, Wilber KP, Gerig G, Gilmore JH. 2003. Comparisons of regional white matter diffusion in healthy neonates and adults performed with a 3.0-T head-only MR imaging unit. Radiology. 229:673–681.